

# Ultra-Light Axion Dark Matter and its impacts on dark halo structure in $N$ -body simulation

Jiajun Zhang

*Department of Physics, The Chinese University of Hong Kong, Hong Kong, China*

Yue-Lin Sming Tsai

*Physics Division, National Center for Theoretical Sciences, Hsinchu, Taiwan*

Kingman Cheung

*Physics Division, National Center for Theoretical Sciences, Hsinchu, Taiwan*

*Department of Physics, National Tsing Hua University, Hsinchu, Taiwan*

*Division of Quantum Phases and Devices, School of Physics, Konkuk University, Seoul 143-701, Republic of Korea*

Ming-Chung Chu

*Department of Physics, The Chinese University of Hong Kong, Hong Kong, China*

## ABSTRACT

The Ultra-Light Axion (ULA) is a dark matter candidate with mass  $\mathcal{O}(10^{-22})$  eV and de Broglie wavelength of order kpc. Such an axion, also called the Fuzzy Dark Matter (FDM), thermalizes via the gravitational force and forms a Bose-Einstein condensate. Recent studies suggested that the quantum pressure from the FDM can significantly affect the structure formation in small scales, thus alleviating the so-called “small-scale crisis”. In this paper, we develop a new technique to discretize the quantum pressure and illustrate the interactions among FDM particles in the  $N$ -body simulation, which accurately simulates the formation of the dark-matter halo and its inner structure. In a self-gravitationally-bound virialized halo, we find a constant density, solitonic core, which is consistent with the theoretical prediction. There are two stable solitonic core sizes, around 1 kpc or 5 kpc. However, the 1 kpc-size core density is higher than the normal CDM density, and vice versa for the 5 kpc-size one. The existence of the solitonic core and double stable solutions reveals the non-linear effect of quantum pressure and impacts the structure formation in the FDM model.

## 1. Introduction

There have been many compelling evidences for the existence of cold dark matter (CDM), which successfully explains the rotational curves of spiral galaxies, the Cosmic Microwave Background power spectrum, the Bullet Cluster, and large scale structure formation of the Universe.

After several decades of efforts to understand the properties of CDM based on gravitational interaction and its role in the evolution of structures, it is still not clear whether CDM is absolutely collisionless without short-range forces such as the weak interaction. The most well-motivated model for CDM is the weakly interacting massive particles (WIMPs), whose mass range is from the sub-GeV to 100 TeV owing to the relic density requirement. Unfortunately, up to now no compelling evidence of WIMPs was found in all different types of searches, such as collider searches Aaboud et al. (2016); CMS (2016), underground detections Akerib et al. (2016); Tan et al. (2016), and astronomical observations Ackermann et al. (2015); Aartsen et al. (2016). Null signals reported in all these experiments have shrunk the parameter space of many WIMP models to some finely-tuned regions. Also, the next generation of CDM searches are shifting their focuses to different mass regions.

The CDM model through detailed  $N$ -body simulations, though successfully explains the observations in large scales, fails to account for the observations in relatively smaller scales; this is known as the "small-scale crisis": (i) the missing satellites problem Moore et al. (1999); Klypin et al. (1999), (ii) the cusp-core problem de Blok (2010), and (iii) the too-big-to-fail problem Boylan-Kolchin et al. (2011). In order to alleviate the problems, a new mechanism of velocity boost is needed for the DM momentum exchanges beyond the collisionless picture of the CDM. Examples include baryonic interaction Schaller et al. (2015a,b), strongly self-interacting DM Tulin et al. (2013), Fuzzy Dark Matter (FDM) Hu et al. (2000), etc. The key point is to smooth out the cuspy matter distribution.

The Ultra-Light Axion (ULA) or so-called Fuzzy Dark Matter (FDM) is then a good candidate for CDM. It not only keeps the success of CDM in dealing with large-scale issues, but also provides a possible solution to the small-scale crisis. The FDM is a scalar boson with an extremely light mass  $\gtrsim 10^{-22}$  eV, which is required by a recent observation on the reionization history of the Universe Bozek et al. (2015). With a common velocity in the order of  $100 \text{ km s}^{-1}$ , the de Broglie wavelength of the FDM is very long  $\sim \mathcal{O}(\text{kpc})$  and the DM of the Universe is a Bose-Einstein condensate (BEC) Sin (1994); Hu et al. (2000); Ferrer & Grifols (2004); Boehmer & Harko (2007); Lee & Lim (2010); Sikivie & Yang (2009); Mielke & Perez (2009); Chavanis (2011); Chavanis & Delfini (2011); Dev et al. (2016) because the BEC transition temperature is higher than the cosmological temperature. Thus, the FDM is still in the non-relativistic regime and behaves like CDM. However, due to the quantum nature of the FDM in small scales, about tens or hundreds of kpc, remarkably the FDM is distinguishable from the normal CDM. One can find those differences in the matter power spectrum Veltmaat & Niemeyer (2016), halo mass function (HMF) Du et al. (2016), and halo structure Schwabe et al. (2016). The most striking feature of the FDM is that the halo has a solitonic core of size  $\sim \mathcal{O}(\text{kpc})$  resulting from the quantum pressure of the FDM particles, which is significantly larger than their self-gravity. Hence, the quantum pressure plays an essential role in solving the small-scale crisis. Moreover, if the halo small scale structure can be measured more accurately in the future, the order of FDM particle mass can be constrained.

In this work, we propose a new scheme – effective Particle-Particle (PP) interaction – for simulating the FDM model, by which one can compute the quantum effect of the FDM in the

$N$ -body simulation with high resolution. In a self-gravitationally-bound virialized halo, we find two stable solutions, both with a constant density core – solitonic core – of size of around 1 kpc or 5 kpc, but with a higher or lower density than the conventional CDM model respectively. The result shows the non-trivial quantum pressure effect on the structure formation. We present the effects of the linear and non-linear power spectrum growth, especially for the non-linear effect in high density regions. For small scale structures, particularly for scales less than one de Broglie wavelength, we find an attractive total potential at high over-density regions. However, in early age, low over-density regions, the linear effect is mainly from the repulsive quantum pressure which suppresses the matter power spectrum at scales smaller than the Jeans scale.

We have made an independent and totally different simulation scheme compared to a few previous studies, which were based on direct cosmological simulations with the Schrödinger-Poisson equations (Schive et al. 2014a) and Particle-Mesh (PM) scheme simulation technique Veltmaat & Niemeyer (2016). We cross-check our results with previous simulations and find them consistent with each other. Nevertheless, our implementation of the quantum effect with a simple PP method helps us to explain some of the previously unclear behavior and understand self-consistently how quantum pressure affects the structure formation.

The following sections are arranged as follows. In Sec. 2, we introduce the theoretical approach of the effective Particle-Particle interaction. In Sec. 3, we describe the the simulation setup and discuss the results. Finally, we summarize our outcomes in Sec. 4.

## 2. Methodology

### 2.1. Schrödinger-Poisson equations

The nature of FDM can be well described by the Schrödinger-Poisson equations,

$$i\hbar \frac{d\Psi}{dt} = -\frac{\hbar^2}{2m_\chi} \nabla^2 \Psi + m_\chi V \Psi, \quad (1)$$

and

$$\nabla^2 V = 4\pi G m_\chi |\Psi|^2. \quad (2)$$

Here  $\hbar$ ,  $m_\chi$  and  $V$  are the Planck constant, particle mass and the gravitational potential acting on a particle, respectively. The wave function  $\Psi$  can be written as

$$\Psi = \sqrt{\frac{\rho}{m_\chi}} \exp\left(\frac{iS}{\hbar}\right) \quad (3)$$

in terms of the number density  $\frac{\rho}{m_\chi}$ , while we can define the gradient of  $S$  to be DM momentum,

$$\nabla S = m_\chi \mathbf{v}. \quad (4)$$

After solving the Schrödinger-Poisson equations, from the real and imaginary parts of the solution, one can obtain the continuity equation,

$$\frac{d\rho}{dt} + \nabla \cdot (\rho \mathbf{v}) = 0, \quad (5)$$

and the momentum-conservation equation,

$$\frac{d\mathbf{v}}{dt} + (\mathbf{v} \cdot \nabla) \mathbf{v} = -\nabla(Q + V), \quad (6)$$

where we have defined the quantum pressure as

$$Q = -\frac{\hbar^2}{2m_\chi^2} \frac{\nabla^2 \sqrt{\rho}}{\sqrt{\rho}}. \quad (7)$$

One can see that such a pressure is only related to the mass density  $\rho$  and can be treated as a new force on the particles additional to gravity. Later, we shall focus on this pressure term and discuss how to obtain the acceleration information by using the Hamiltonian field theory.

To discuss the effect of the quantum pressure, we can start with the Hamiltonian without the gravity term,

$$H = \int \frac{\hbar^2}{2m_\chi} |\nabla \Psi|^2 d^3x = \int \frac{\rho}{2} |\mathbf{v}|^2 d^3x + \int \frac{\hbar^2}{2m_\chi^2} (\nabla \sqrt{\rho})^2 d^3x. \quad (8)$$

We can write the kinetic energy term in discretized form with object index  $j$

$$T = \int \frac{\rho}{2} |\mathbf{v}|^2 d^3x = \sum_j \frac{1}{2} m_j \left( \frac{dq_j}{dt} \right)^2, \quad (9)$$

where  $q_j$  is the coordinate of the  $j$ th particle, and the effective potential energy is from the quantum pressure

$$K_\rho = \int \frac{\hbar^2}{2m_\chi^2} (\nabla \sqrt{\rho})^2 d^3x. \quad (10)$$

Note that we did not discretize  $K_\rho$  here but delay it to the next subsection because it will require some efforts to do so. Based on  $T$  and  $K_\rho$  the Lagrangian of the system without gravity is

$$L = T - K_\rho = \sum_j \frac{1}{2} m_j \left( \frac{dq_j}{dt} \right)^2 - \int \frac{\hbar^2}{2m_\chi^2} (\nabla \sqrt{\rho})^2 d^3x, \quad (11)$$

and the Euler-Lagrangian equation becomes

$$\frac{d}{dt} \frac{\partial L}{\partial \dot{q}_j} - \frac{\partial L}{\partial q_j} = 0 \implies m_j \ddot{q}_j = -\frac{\partial K_\rho}{\partial q_j}. \quad (12)$$

One can see that the  $\rho$  in  $K_\rho$  is a continuous function, which cannot be used in the PP method. Therefore, the major task is to further discretize the continuous function  $\partial K_\rho / \partial q_j$ , which we shall describe in more details in the next subsection.

## 2.2. Particle-particle implementation of quantum pressure

For a particle-particle interaction system, the number density for each individual particle is a delta function. Intuitively, the mass density  $\rho$  can be discretized as

$$\rho(\mathbf{r}) = \sum_i m_i \delta(\mathbf{r} - \mathbf{r}_i), \quad (13)$$

where the summation over the index  $i$  means to add up all the particles. Numerically, treatment of a delta function may cause a difficult computational problem because of the sampling coverage issue. However, conventionally one can approximate a delta function as a narrow Gaussian/kernel function, as long as the width is small enough. The reasons and advantages to use the Gaussian smoothing kernel are listed as follows. (i) It naturally keeps the kernel smooth, differentiable, and spherically symmetric. (ii) In quantum physics the Gaussian kernel is the eigenstate of the wavefunction inside a parabolic potential well. (iii) Finally, if we were to use the spline kernel instead, there would be a singularity at the particle position. Because of the finite grid size, such a singularity can numerically make the results unphysical. Specifically, we write down the form of the delta function as

$$\delta(\mathbf{r} - \mathbf{r}_i) = \frac{1}{2\sqrt{2}\lambda^3\pi^{3/2}} \exp\left(-\frac{2|\mathbf{r} - \mathbf{r}_i|^2}{\lambda^2}\right), \quad (14)$$

with a narrow width  $\lambda$ . Note that the value of  $\lambda$  is not an arbitrary and should be the same as the de Broglie wavelength because one FDM particle has to be found with a high probability within a Gaussian wave packet. In our work, the probability of finding a FDM in one wavelength is set at 95%.

Taking the FDM mass around  $\mathcal{O}(10^{-31})$  GeV as an example, its wavelength  $\lambda$  is order of kpc. Inserting Eq. (14) back to the  $(\nabla\sqrt{\rho})^2$  term in Eq. (10), the expression can be expanded by using the kernel function,

$$\begin{aligned} \left[\nabla\sqrt{\rho(\mathbf{r})}\right]^2 &= \frac{1}{4\rho(\mathbf{r})} \left[ \sum_i m_i \nabla \delta(\mathbf{r} - \mathbf{r}_i) \right]^2, \\ &= \frac{1}{4\rho(\mathbf{r})} \left[ \sum_i m_i \delta(\mathbf{r} - \mathbf{r}_i) \left(-\frac{4}{\lambda^2}\right)(\mathbf{r} - \mathbf{r}_i) \right]^2, \\ &= \frac{4}{\lambda^4\rho(\mathbf{r})} \left[ \sum_i m_i \delta(\mathbf{r} - \mathbf{r}_i)(\mathbf{r} - \mathbf{r}_i) \right]^2. \end{aligned} \quad (15)$$

In the simulation, those FDM particles such as axions will be grouped into a big mass clump in space which can be treated as an imaginary particle point (neglecting the size of the clump in the cosmological scale), and the mass density, Eq. (13), becomes

$$\rho(\mathbf{r}) = \sum_j \sum_i m_i \delta(\mathbf{r} - \mathbf{r}_j), \quad (16)$$

with the index  $j$  for each imaginary particle clump. Mathematically, one can think that the mass density is expanded around  $\mathbf{r}_j$  to include all the FDM particles,  $\mathbf{r} \rightarrow \mathbf{r} - \mathbf{r}_j$  and  $\mathbf{r}_i \rightarrow \mathbf{r}_i - \mathbf{r}_j$ . Given such a consideration, the summation of individual FDM particles is effectively the same as summing over all the imaginary particle points, and Eq. (15) can be further polished to be

$$\left[ \nabla \sqrt{\rho(\mathbf{r})} \right]^2 \simeq \frac{4}{\lambda^4} \left[ \sum_j m_j \delta(\mathbf{r} - \mathbf{r}_j) (\mathbf{r} - \mathbf{r}_j) \right]^2 \left[ \sum_j m_j \delta(\mathbf{r} - \mathbf{r}_j) \right]^{-1}. \quad (17)$$

It is worth mentioning that the form in Eq. (17) is identical to Eq. (15) but their meanings should not be confused. Hence, we leave the different indices here. At this stage, we have successfully converted the Gaussian wave packet into an imaginary particle-smoothing kernel.

To completely discretize  $\partial K_\rho / \partial q_j$ , we still need to integrate Eq. (17) over all space. Due to the nature of the delta function, we just need to focus on the volume surrounding the imaginary particle points. Therefore, the integration together with kernel approach gives

$$\int \left[ \nabla \sqrt{\rho(\mathbf{r})} \right]^2 dx^3 \simeq \int \frac{4dx^3}{\lambda^4} \left[ \sum_j m_j \delta(\mathbf{r} - \mathbf{r}_j) (\mathbf{r} - \mathbf{r}_j) \right]^2 \left[ \sum_j m_j \delta(\mathbf{r} - \mathbf{r}_j) \right]^{-1} \quad (18)$$

$$\simeq 4\lambda^{-4} \sum_j m_j \delta(\mathbf{r} - \mathbf{r}_j) (\mathbf{r} - \mathbf{r}_j)^2 \Delta V_j \quad (19)$$

$$\simeq 4\lambda^{-4} \sum_j m_j \frac{\Delta V_j}{\lambda^3 \pi^{3/2}} \exp \left[ -\frac{(\mathbf{r} - \mathbf{r}_j)^2}{\lambda^2} \right] (\mathbf{r} - \mathbf{r}_j)^2, \quad (20)$$

where  $\Delta V_j$  is an effective volume of the simulation particle  $j$ . Numerically, the factor  $\frac{\Delta V_j}{\lambda^3 \pi^{3/2}}$  is of order one since the parameter  $\Delta V_j$  cannot be much different from  $\lambda^3$ . Therefore, this gives us a constrain on the simulation setting. We shall set up the simulation so that every simulation particle occupies a volume close to  $\lambda^3$  in physical coordinates.

Finally, Eq. 10 can be simply rearranged as

$$\sum_j \frac{\partial K_\rho}{\partial q_j} = \frac{4\hbar^2}{m_\chi^2 \lambda^4} \sum_j m_j \Delta V_j \exp \left[ -\frac{2|\mathbf{r} - \mathbf{r}_j|^2}{\lambda^2} \right] \left( 1 - \frac{2|\mathbf{r} - \mathbf{r}_j|^2}{\lambda^2} \right) (\mathbf{r} - \mathbf{r}_j), \quad (21)$$

and the equation of motion, Eq. (12), becomes

$$\sum_j m_j \ddot{\mathbf{q}} = -\frac{4\hbar^2}{m_\chi^2 \lambda^4} \sum_j m_j \Delta V_j \exp \left[ -\frac{2|\mathbf{r} - \mathbf{r}_j|^2}{\lambda^2} \right] \left( 1 - \frac{2|\mathbf{r} - \mathbf{r}_j|^2}{\lambda^2} \right) (\mathbf{r} - \mathbf{r}_j). \quad (22)$$

Substituting  $q$  with  $\mathbf{r}$ , the additional acceleration from quantum pressure used in the simulation can be written as

$$\ddot{\mathbf{r}} = \frac{4M\hbar^2}{M_0 m_\chi^2 \lambda^4} \sum_j \exp \left[ -\frac{2|\mathbf{r} - \mathbf{r}_j|^2}{\lambda^2} \right] \left( 1 - \frac{2|\mathbf{r} - \mathbf{r}_j|^2}{\lambda^2} \right) (\mathbf{r}_j - \mathbf{r}). \quad (23)$$

Here  $M$  is the mass of the simulation particle and  $M_0$  is a normalization factor accounting for the size of  $\Delta V_j$ , which we choose to be  $10^6 M_\odot$ . Interestingly, if we put any “one” test particle around some quantum pressure sources, the additional energy to the system injected from quantum pressure term is zero. Namely, the total work, the integration of Eq. (23) from  $r = 0$  to  $r = \infty$ , vanishes.

To illustrate the effect of quantum pressure, let us consider a two-particle system separated by a distance of order  $\mathcal{O}(\text{kpc})$  and the acceleration caused by quantum pressure will be  $\mathcal{O}(\frac{\hbar^2}{m^2 \lambda^3}) \sim \mathcal{O}(10^{-10} m/s^2)$ . In the left panel of Fig. 1, we demonstrate the effect of quantum pressure in the plane of  $(r, \ddot{r})$ . The acceleration from quantum pressure, gravity, and the sum are shown by black dashed line, blue line, and red line, respectively. Clearly, the quantum pressure can be attractive force (positive sign in our definition) if the distance between two particles is less than  $\lambda/\sqrt{2}$ . However, it becomes a repulsive force (negative sign in our definition) if the distance is greater than  $\lambda/\sqrt{2}$ . To understand this, we refer back to the quantum pressure definition in Eq. (7). The pressure term  $Q$  is proportional to the second derivative of the mass density, namely, the curvature of the density, which can have negative, positive, or zero values, physically corresponding to attractive, repulsive, and zero forces.

In the right panel of Fig. 1, we show the position  $x(t)$  of one of the particles in this two-particle system as a function of time by solving Eq. (23). Here the origin is located at the center of mass and such that  $r(t) = 2x(t)$ . The red-solid, black-dashed, green-solid, and blue-dash-dotted lines present the cases with the initial position  $x(0)$  at  $0.3\lambda$ ,  $\lambda/\sqrt{8}$ ,  $0.4\lambda$ , and  $2\lambda$ , respectively. Also, the position of the other particle is drawn in the corresponding lighter colors for reference. Interestingly, when the distance between the two particles is smaller than  $\lambda/\sqrt{2}$ , the attractive force will bound them. Note that this also demonstrates the phenomenon of Bose-Einstein condensation. One shall bear in mind that for fermionic particles such short range attractive forces would not exist because of the Pauli-exclusion principle. However, the repulsive force will push these two particles away for  $\frac{\lambda}{\sqrt{2}} < r(0) < \sqrt{2}\lambda$ . At  $r(0) = \lambda/\sqrt{2}$ , the node presents the zero interaction. For the  $x(0) \gg \sqrt{2}\lambda$  case, the two particles barely feel the force from each other so that they will continue with their initial velocities, though we set them to be zero.

This reveals the quantum pressure as a short-range interaction, shown in Eq. (23), in the exponentially decaying term.

### 3. Numerical result

**Gadget2** Springel (2005) is a **TreePM** hybrid N-body code. However, in order to describe continuous quantum pressure, the interaction term has to be discretized as we have discussed in the previous section. Therefore, we modified **Gadget2** to compute the contribution from the quantum pressure. In this section, we first describe the details of what we used in our simulation, and then we present our simulation results.

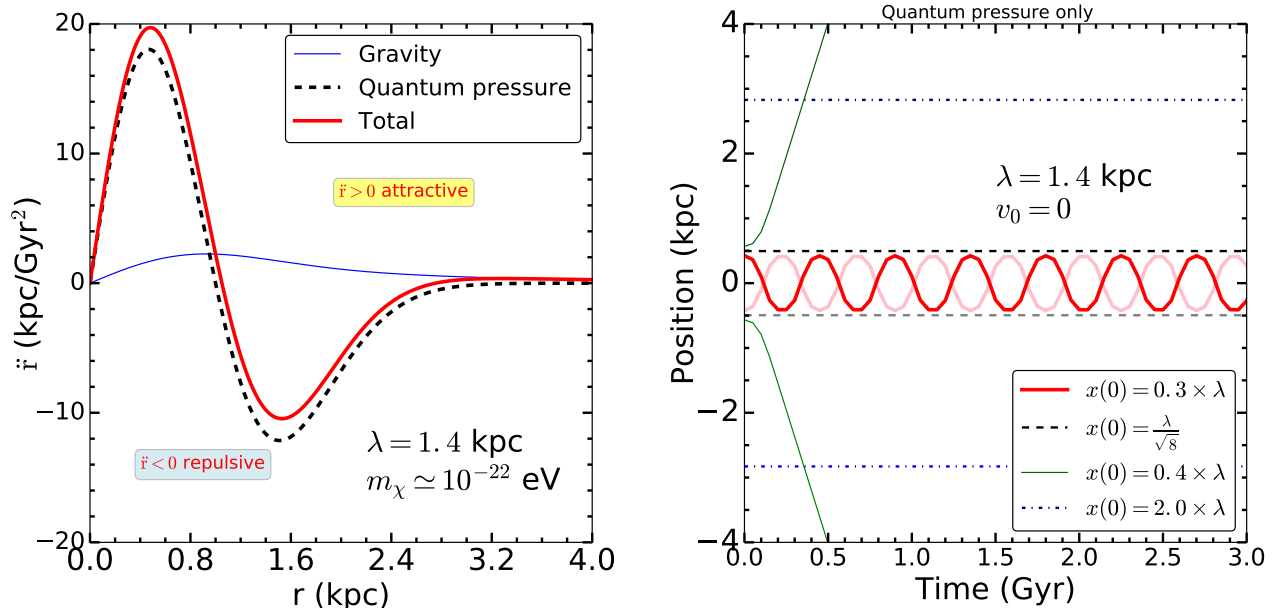


Fig. 1.— Left panel: the acceleration from quantum pressure (black dashed), gravity (blue solid), and their sum (red solid) between two particles. The x-axis is the distance between two particles while the y-axis is the acceleration. Right panel: the particle position, which is changing due to the quantum pressure, vs time. The red-solid, black-dashed, green-solid, and blue-dash-dotted lines present the initial positions at  $0.3\lambda$ ,  $\lambda/\sqrt{8}$ ,  $0.4\lambda$ , and  $2\lambda$ , respectively. However, the light color lines represent their partner particles located at the opposite side  $-0.3\lambda$ ,  $-\lambda/\sqrt{8}$ ,  $-0.4\lambda$ , and  $-2\lambda$  initially.



### 3.1. The simulation setup

The PM method is mostly useful for cosmological simulations with periodic boundary conditions. As we have seen from the previous section that the quantum pressure behaves like a short-range interaction, we therefore keep the original PM code which takes care of the long-range force calculation. However, we have to use the Tree method to take care of the short-range force calculation, namely, the force calculation basis for **Gadget2**. Hence, the part of Tree force calculation in **Gadget2** has to be modified to include the quantum pressure term. Finally, we do not need to set softening for the quantum pressure acceleration since it is finite in the  $(\mathbf{r}_j - \mathbf{r}) \simeq 0$  region.

To study the differences between the CDM and FDM, we set up a self-collapsing system. A cubic box with a side length 400 kpc is generated with totally  $10^6$  simulation particles homogeneously distributed inside the box. Each simulation particle consists of a  $10^6$  solar mass. All particles start from rest and the system collapses resulting from their self-gravity to form a stable self-gravitationally-bound virialized halo at the center. It is sufficient to stop the simulation around 10 Gyr. The final stable virialized halo in FDM model depends sensitively on the initial slight perturbation given to the system.

Two kinds of **Gadget2** simulations are performed: one with the modified code for FDM quantum pressure effect and the other one with the original **Gadget2** code. In both simulations, we use the same initial conditions, and the gravitational softening length is chosen to be 0.8 kpc. The ULA mass and wavelength are fixed to be  $2.5 \times 10^{-22}$  eV and 1.4 kpc, respectively. We further run several simulations with different softening lengths in order to make sure that the final density and velocity distributions of the halos have converged.

### 3.2. Simulation results

In Fig. 2, we present the particle distributions of our simulations for a self-gravitationally-collapse system. The three panels on the upper row are for the CDM scenario while the other three on the lower row are for the FDM case. The figures from the left to right panels are two-dimensional slices at the evolution time 0, 2, and 3 Gyr. Clearly, the distribution of FDM is more smooth and spread out than the CDM case, especially at the later time. This is exactly the novel feature of the quantum pressure.

To further illustrate the effect of the quantum pressure on the halo density profile, we plot the mass enclosed in 8 kpc in the left panel of Fig. 3, which shows the core mass evolution along the time direction in the unit of Gyr for the CDM case (blue line) and for the FDM (red solid line for the first solution, FDM1, and red dashed line for the second solution, FDM2). Both systems of CDM and FDM will be in the equilibrium state after 3 – 4 Gyr when the mass density with 8 kpc does not change significantly. Note that the time scale to achieve the equilibrium state still depends on the gravitational potential but the first (second) solution of FDM halo possesses slightly less mass inside 8 kpc than (about one half of mass inside 8 kpc as) the CDM one, due to the the

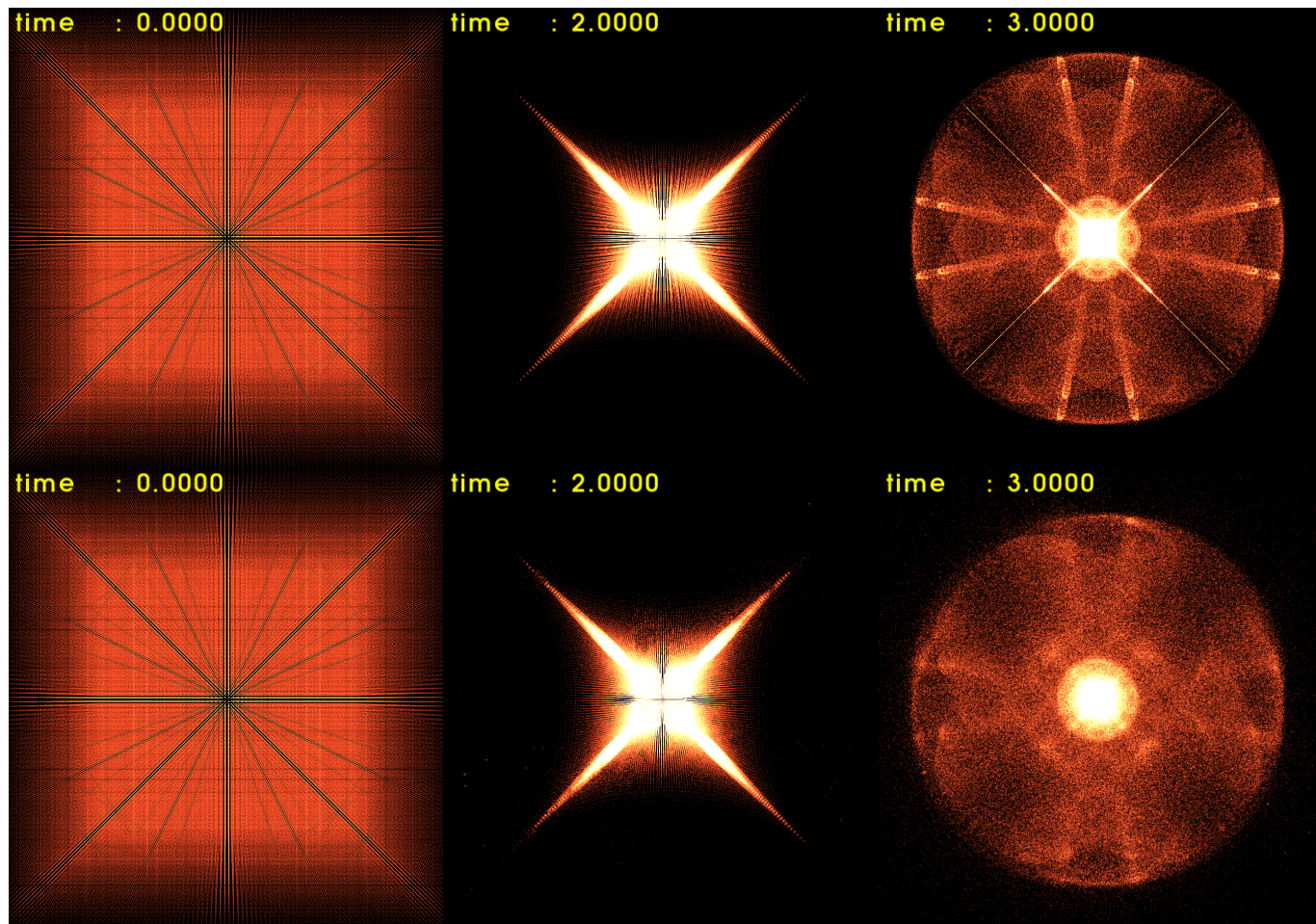


Fig. 2.— The particle distributions of the CDM (on the top) and FDM (on the bottom) simulations for a self-gravitationally-collapse system. The labels at the upper left corner show the time in Gyr.

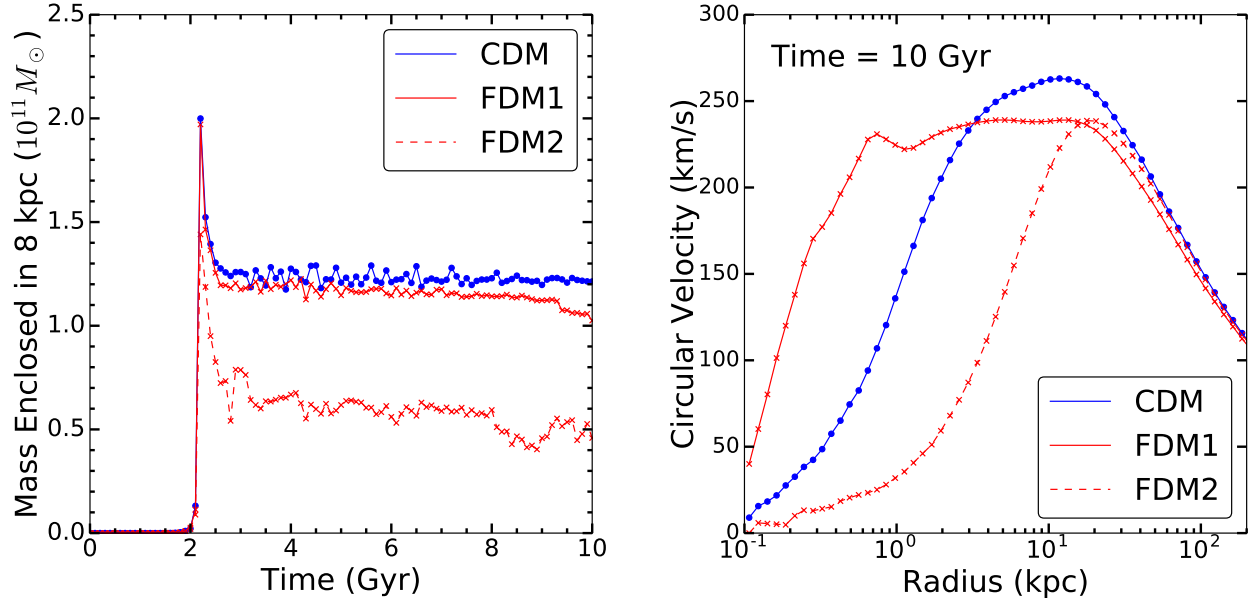


Fig. 3.— The evolution of mass enclosed in 8 kpc from the center is shown on the left panel. After 3 – 4 Gyr evolution, the self-collapse system reaches equilibrium for both CDM and FDM models. The right panel shows the final rotational curve. The circular velocity for the first solution of FDM is larger than the CDM inside 3 kpc from the center but smaller outside 3 kpc, while that for the second solution of FDM is always smaller than the CDM.

quantum pressure. The FDM halo for both solutions are slowly losing mass inside 8 kpc even after 4 Gyr while the CDM is already stable.

In the right panel of Fig. 3, we show the rotational curves for the FDM (red solid line for FDM1 and red dashed line for FDM2) and CDM (blue line) halo after 10 Gyr evolution. We take this halo as an example because it is fully virialized. We can see that inside 3 kpc the circular velocity for the FDM1 halo is larger than that of the CDM halo but smaller for outside 3 kpc. On the other hand, the FDM2 halo always gives a smaller circular velocity than that of the CDM halo. This implies that the FDM1 halo has a higher density in the inner core than that of the CDM, while the FDM2 halo has a lower density. Note that a small bump around 1 kpc of the FDM1 rotational curve marks the transition point of the quantum pressure from being attractive to repulsive.

We plot two density profiles at 3 Gyr and 10 Gyr separately in Fig. 4. In the left panel, we show the density profiles for the FDM (red diamonds and crosses) and CDM (blue circles) halos at 3 Gyr. The halo is still not reaching the equilibrium at 3 Gyr time, and there are no significant differences between the CDM and FDM, except that the second solution of the FDM indicates lower densities within 3 kpc. We also plot the Einasto Profile fitting in the final virialized state in blue dashed line for comparison. At the region around 100 kpc, some particles are still bouncing out so that the tail is not fitted well to the Einasto profile. In the right panel, we show the density profiles at 10 Gyr. Two fitting functions of solitonic cores are shown in red-dashed line, whose formula was given in Ref. Schive et al. (2014b),

$$\rho_c(r) \simeq \rho_b \rho_0 [1 + 0.091 (\frac{r}{r_c})^2]^{-8}, \quad (24)$$

with an additional fitting parameter  $\rho_b$ , and

$$\rho_0 \simeq 3.1 \times 10^6 (\frac{2.5 \times 10^{-22} \text{ eV}}{m_\chi})^2 (\frac{\text{kpc}}{r_c})^4 \frac{M_\odot}{\text{kpc}^3}. \quad (25)$$

We set  $\rho_b = 150$  and  $r_c = 0.4$  in our plot for the first solution,  $\rho_b = 60000$  and  $r_c = 8.0$  for the second solution. Beyond the solitonic core, the density profiles of FDM halos are essentially the same as that of CDM and the Einasto profile.

We confirm the existence of two possible solitonic cores, slowly emerging from the FDM simulation, but the density of FDM1 is higher than that of the CDM halo inside 1 kpc due to the attractive quantum pressure, that of FDM2 is lower than that of the CDM halo due to the repulsive quantum pressure outside 1 kpc. In a previous study Veltmaat & Niemeyer (2016), a boost power in small scale was also reported for their small-box comoving coordinate simulation. Comparing to the CDM simulation, Ref. Veltmaat & Niemeyer (2016) found at most 10% more power in the FDM simulation. We can now easily understand such a result by considering the attractive quantum pressure in small scales with the help of our PP approach.

We also compare the velocity dispersion profiles of the FDM (red lines) and CDM (blue line) halos after 3 Gyr (left panel) and after 10 Gyr (right panel) of evolution in Fig. 5. At 3 Gyr (left panel), we do not see significant differences between the FDM1 and CDM halos, except in a small

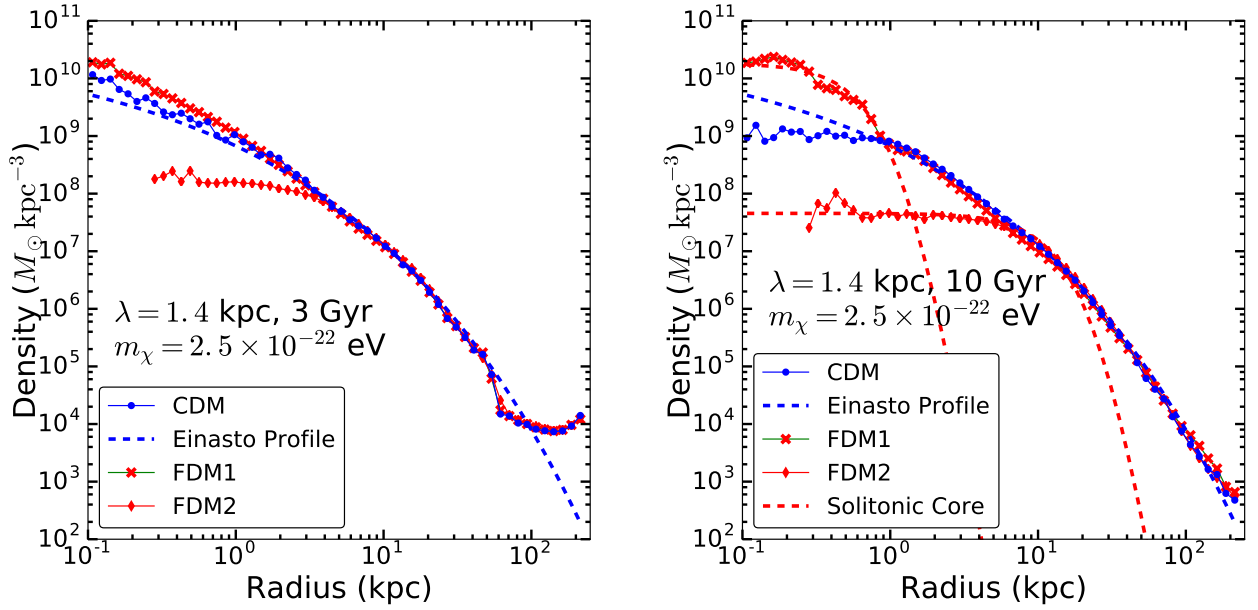


Fig. 4.— The left (right) panel is the halo density profile after 3 (10) Gyr. The system is fully virialized after 10 Gyr. We can see that the FDM and CDM halo density profiles outside 10 kpc can both be fitted well by the Einasto profile. However, inside 1 kpc a solitonic core slowly emerges in the FDM1 halo and its density is higher than that of CDM since the quantum pressure inside 1 kpc is attractive. For the FDM2 halo, the density is lower than that of CDM halo after 3 Gyr and finally evolves into a solitonic core inside 10 kpc.

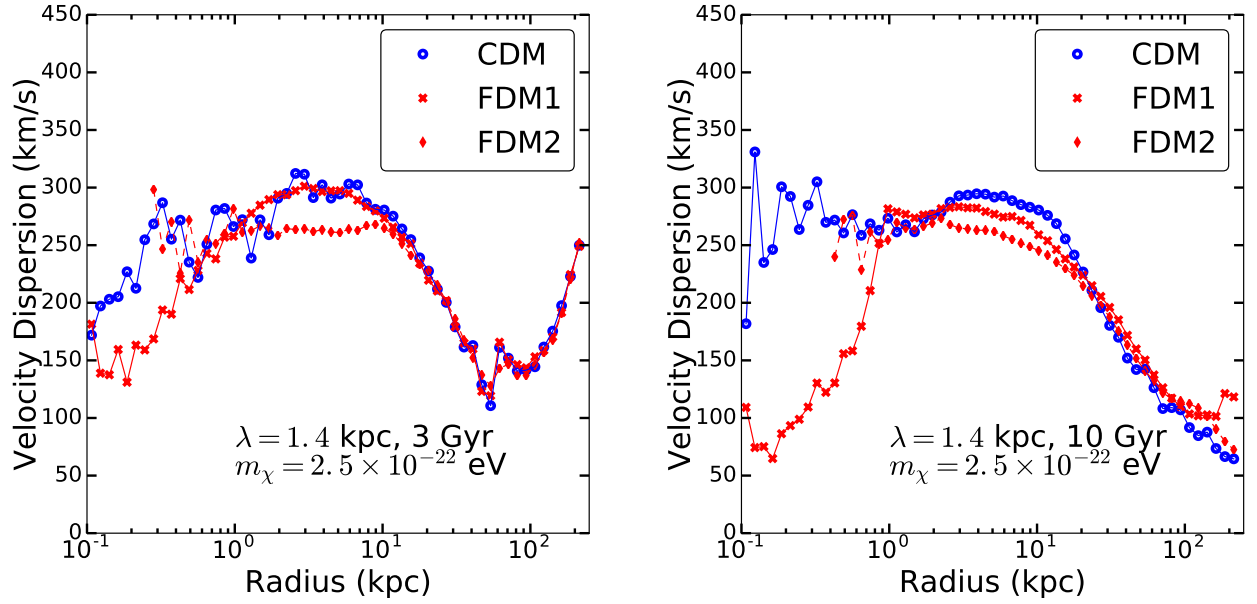


Fig. 5.— Left(right) panel: the velocity dispersion profiles at 3(10) Gyr. Before final virialization, one cannot find significant difference between the FDM1 and CDM halos, but for FDM2, the velocity dispersion is distinguishable from that of the CDM halo inside 10 kpc. The velocity dispersion for the FDM1 halo at 10 Gyr is much smaller than that of the CDM halo at the region less than 1 kpc, while for the FDM2 halo, there are too few particles inside 1 kpc to provide convincing measurement. The slight differences among the CDM, FDM1 and FDM2 halos around 10 kpc are still clear.

central region less than 0.4 kpc. However, the FDM1 solitonic core region (within 1 kpc) at 10 Gyr shows a much smaller velocity dispersion than the CDM, and a slightly smaller velocity dispersion between 3 kpc and 20 kpc for the FDM1 halo. The FDM2 halo is rather different from the FDM1 and CDM halos at 3 Gyr; its velocity dispersion is smaller than that of CDM halo between 3 kpc and 20 kpc, both at 3 kpc and at 10 Gyr. We can understand that owing to less mass enclosed within 3 kpc, the two solutions of the FDM halos have smaller velocity dispersion than that of the CDM halo, as discussed in Fig. 3.

#### 4. Summary and outlook

In summary, we have proposed to use a Gaussian kernel function to discretize the quantum pressure term to simulate FDM in the PP method for  $N$ -body simulations. We note that the quantum pressure does not provide additional energy to the system, but it will certainly change the halo inner structure. In order to understand the quantum pressure effect, we study a two-body system and find that the force between the two particles is always attractive if the distance between them is less than  $\lambda/\sqrt{2}$ , but it will turn repulsive if the distance between them is larger than  $\lambda/\sqrt{2}$ . In small scales, the quantum pressure contribution can be even larger than gravity. We have also shown that the BEC properties can be quantitatively understood by using our discretized quantum pressure equation.

With our discretized quantum pressure approach to the PP method, we have constructed two  $N$ -body simulations, one for the CDM and the other one for the FDM, in a collapsing system with identical initial conditions. We found that the FDM halo center can be clearly distinguished from that of the CDM and also confirmed that a solitonic core forms at the FDM halo center, where the mass density is very flat, similar to the isothermal or Burkert profiles.

We have also compared the FDM halo evolution with the CDM case based on the mass enclosed within 8 kpc. We confirmed that the FDM halo will reach equilibrium slightly later than the CDM one while its galaxy formation history is consistent with current data Hui et al. (2016).

Implied from the rotation curves, the FDM halo evolves into an inner solitonic core with either higher or lower density than the CDM if they started with identical initial condition; similar results can also be found in Ref. Veltmaat & Niemeyer (2016).

The solitonic core we found in this work may not be able to fully solve the cusp-core problem, but it is very suggestive that it may provide a solution if a full scale cosmological simulation is performed. One may worry that the non-linear effect from the attractive quantum pressure at the region less than one wavelength scale can bring higher mass density back to the center. This can be understood as the linear power-spectrum growth from the FDM model suppresses any power smaller than the FDM Jeans scale

$$\frac{2(\pi G \rho)^{1/4} m_\chi^{1/2}}{\hbar^{1/2}}.$$

However, we started our simulations for the CDM and FDM from the identical initial conditions,

and the quantum pressure of the FDM suppresses the density for scales larger than one wavelength albeit boosts the density up in scales smaller than one wavelength. These two effects were also found in Ref. Veltmaat & Niemeyer (2016) – the suppression of matter power spectrum from redshift  $z = 100$  to  $z = 16$  in small scales, but a boost of matter power spectrum at around  $z = 2$  in small scales.

Also notice two different solutions for the FDM halo which are stable, one with a denser and smaller core while the other one with a lower density but larger core. These two solutions might both exist in the Universe, while the larger core may account for the cusp-core problem. We leave the discussion about these two solutions and more detailed explanation of them to the future work.

We do not consider the cosmological simulation in this work but would like to return to this in the near future.

### Acknowledgment

We acknowledge the help from ITSC in CUHK for providing computational resources for the project. This project is supported partially by grants from the Research Grant Council of the Hong Kong Special Administrative Region, China (Project No. C4047-14E) and the VC Discretionary Fund of CUHK. K.C. was supported by the MoST under Grants No. MOST-105-2112-M-007-028-MY3.

### REFERENCES

- Aaboud, M., et al. 2016, Phys. Rev., D94, 032005
- Aartsen, M. G., et al. 2016, Eur. Phys. J., C76, 531
- Ackermann, M., Albert, A., Anderson, B., et al. 2015, Physical review letters, 115, 231301
- Akerib, D. S., et al. 2016, arXiv:1608.07648
- Boehmer, C. G., & Harko, T. 2007, JCAP, 0706, 025
- Boylan-Kolchin, M., Bullock, J. S., & Kaplinghat, M. 2011, Mon. Not. Roy. Astron. Soc., 415, L40
- Bozek, B., Marsh, D. J., Silk, J., & Wyse, R. F. 2015, Monthly Notices of the Royal Astronomical Society, 450, 209
- Chavanis, P.-H. 2011, Physical Review D, 84, 043531
- Chavanis, P.-H., & Delfini, L. 2011, Physical Review D, 84, 043532
- CMS. 2016



- de Blok, W. J. G. 2010, *Adv. Astron.*, 2010, 789293
- Dev, P., Lindner, M., & Ohmer, S. 2016, arXiv preprint arXiv:1609.03939
- Du, X., Behrens, C., & Niemeyer, J. C. 2016, arXiv preprint arXiv:1608.02575
- Ferrer, F., & Grifols, J. A. 2004, *JCAP*, 0412, 012
- Hu, W., Barkana, R., & Gruzinov, A. 2000, *Phys. Rev. Lett.*, 85, 1158
- Hui, L., Ostriker, J. P., Tremaine, S., & Witten, E. 2016, arXiv:1610.08297
- Klypin, A. A., Kravtsov, A. V., Valenzuela, O., & Prada, F. 1999, *Astrophys. J.*, 522, 82
- Lee, J.-W., & Lim, S. 2010, *JCAP*, 1001, 007
- Mielke, E. W., & Perez, J. A. V. 2009, *Phys. Lett.*, B671, 174
- Moore, B., Ghigna, S., Governato, F., et al. 1999, *Astrophys. J.*, 524, L19
- Schaller, M., Frenk, C. S., Bower, R. G., et al. 2015a, *Mon. Not. Roy. Astron. Soc.*, 451, 1247
- . 2015b, *Mon. Not. Roy. Astron. Soc.*, 452, 343
- Schive, H.-Y., Chiueh, T., & Broadhurst, T. 2014a, *Nature Physics*, 10, 496
- Schive, H.-Y., Liao, M.-H., Woo, T.-P., et al. 2014b, *Physical review letters*, 113, 261302
- Schwabe, B., Niemeyer, J. C., & Engels, J. F. 2016, *Physical Review D*, 94, 043513
- Sikivie, P., & Yang, Q. 2009, *Phys. Rev. Lett.*, 103, 111301
- Sin, S.-J. 1994, *Phys. Rev.*, D50, 3650
- Springel, V. 2005, *Monthly Notices of the Royal Astronomical Society*, 364, 1105
- Tan, A., Xiao, M., Cui, X., et al. 2016, *Physical Review Letters*, 117, 121303
- Tulin, S., Yu, H.-B., & Zurek, K. M. 2013, *Phys. Rev.*, D87, 115007
- Veltmaat, J., & Niemeyer, J. C. 2016, arXiv preprint arXiv:1608.00802